

Adversarial Numerical Analysis for Inverse Problems[☆]

Kailai Xu^a, Eric Darve^{a,b}

^a*Institute for Computational and Mathematical Engineering, Stanford University, Stanford, CA, 94305*

^b*Mechanical Engineering, Stanford University, Stanford, CA, 94305*

Abstract

Many scientific and engineering applications are formulated as inverse problems associated with stochastic models. In such cases the unknown quantities are distributions. The applicability of traditional methods is limited because of their demanding assumptions or prohibitive computational consumptions; for example, maximum likelihood methods require closed-form density functions, and Markov Chain Monte Carlo needs a large number of simulations. We introduce adversarial numerical analysis, which estimates the unknown distributions by minimizing the discrepancy of statistical properties between observed random process and simulated random process. The discrepancy metric is computed with a discriminative neural network. We demonstrated numerically that the proposed methods can estimate the underlying parameters and learn complicated unknown distributions.

Keywords: Adversarial Training, Neural Networks, Automatic Differentiation

1. Introduction

Almost all model-based problems in data analytics and scientific computing can be classified into two categories: forward problems and inverse problems. The forward problems assume that models and parameters—such as boundary conditions in partial differential equations—are explicitly given and ask for model outputs. However in the inverse problem, part of the parameters in the models are unknown but we observe (partial) outputs. The unknown parameters are calibrated based on stochastic models and observations. Among inverse problems, those associated with stochastic models are particularly interesting since stochasticity is indispensable for modeling real-world phenomenon. In the following we discuss several examples for inverse modeling with stochasticity

- In **uncertainty quantification**, we have a partial differential equation (PDE) model

$$\begin{aligned} \mathcal{L}_\theta u(x) &= 0 & x \in \Omega \\ \mathcal{B}u(x) &= 0 & x \in \partial\Omega \end{aligned} \tag{1}$$

Email addresses: kailaix@stanford.edu (Kailai Xu), darve@stanford.edu (Eric Darve)

where \mathcal{L}_θ is a differential operator parametrized by an unknown θ , and \mathcal{B} is the operator associated with the boundary condition. Due to the stochastic nature of the physical process, θ is not deterministic and subject to an unknown distribution \mathcal{P} . Therefore, the resultant solution u is a random variable. Given multiple observations u_i for u , how can we reconstruct the unknown distribution \mathcal{P} ?

- In the **stochastic heat equation**

$$\partial_t u(t, x) = \nabla \cdot (\theta \nabla u(t, x)) + \xi, (t, x) \in \mathbb{R}_+ \times \mathbb{R}^d \quad (2)$$

where ξ is a centered Gaussian process such that $\mathbb{E}\xi(s, x)\xi(t, y) = \delta(t-s)\delta(x-y)$ (δ is the Dirac delta function). We have observed $u(t_i, x_i)$ at multiple times and locations, $i = 1, 2, \dots, n$ and want to estimate the unknown conductivity coefficient $\theta \in \mathbb{R}^{d \times d}$ from those observed data.

- In **finance**, the stochastic differentiation equations can be used for modeling interest rates. For example, the square root process given by

$$dr_t = \alpha(\mu - r_t)dt + \sqrt{r_t}\sigma dW_t \quad (3)$$

where r_t is the interest rate, $\{W_t, t \geq 0\}$ is a standard Brownian motion and $\theta = (\alpha, \mu, \sigma)$ are model parameters. To describe the dynamics of the interest rates, one can calibrate the parameters θ based on discrete observations $r_{t_1}, r_{t_2}, \dots, r_{t_n}$ at time $t = t_1, t_2, \dots, t_n$.

However, despite wide applications of inverse problems associated with stochastic models, they are challenging to solve and remain largely unexplored in the literature (compared to their *deterministic* model counterparts). When the distributions in the models are non-Gaussian, there are few analytical tools available and therefore we must resort to numerical analysis. Traditionally, numerical methods have been mostly developed for inverse problems associated with deterministic models or Gaussian-based stochastic models. There are only a few approaches for non-Gaussian cases and their applicability is limited (see the following text).

Before we review traditional methods and describe our approach, we first formulate Eqns. (1) to (3) by a unified mathematical model. Assume that w is sampled from a known stochastic process and θ is a random variable with an unknown distribution. The governing equation for the system is

$$x = F(w, \theta) \quad (4)$$

The output, x , will also be a random variable or process. Our task is to estimate the distribution of θ , \mathcal{P} , from observations $\{x_i\}_{i=1}^n$. Even though the random process from which w is sampled is known, w itself is not observable; this is common in many applications. Table 1 discusses the corresponding w , θ and x in previous examples.

We now have a brief review of traditional methods for inverse modeling of Eq. (4) and below is their challenges and limitations. We will discuss two cases separately

Example	w	θ	\mathcal{P}	x
Uncertainty Quantification	–	θ	Unspecified	$u(x)$
Stochastic Heat Equation	ξ	conductivity θ	δ_θ	$u(t, x)$
Stochastic Differential Equation	W_t	(α, μ, σ)	$\delta_\alpha \delta_\mu \delta_\sigma$	r_t

Table 1: The known random process w , unknown random variable θ and the corresponding distribution \mathcal{P} , and the output x . In the probability column, “Unspecified” means the form of the probability distribution is not specified, and δ_θ means the Dirac delta distribution.

1. $\mathcal{P} = \delta_{\theta^*}(\theta)$ is a Dirac Delta distribution for an unknown θ^* .
2. The form of the distribution \mathcal{P} of θ is not given; in this case, \mathcal{P} can be approximated by a parametrized functional form and hence the problem is reduced to the last case.

When $\mathcal{P} = \delta_{\theta^*}(\theta)$ is a Dirac Delta distribution for an unknown θ^* , the inverse problem for eq. (4) is reduced to the parameter estimation problem. The traditional starting point of estimating θ is the maximum likelihood estimator, which maximizes the log-likelihood function

$$\max_{\theta} l_{\theta}(x_1, x_2, \dots, x_N) := \sum_{i=1}^N \log p(x_i | \theta) \quad (5)$$

where $\{x_i\}_{i=1}^N$ are observed samples from the random process x . The maximum likelihood method (MLE) is provably asymptotically efficient, that is, consistent and asymptotically normal with variance equal to the Cramér-Rao lower bound under certain conditions; typical conditions are given in [1–3]. However, MLE requires computing $p(x_i | \theta)$. When F is a very complicated model, it is difficult to obtain the analytical form of $p(x_i | \theta)$ or compute it numerically.

In the general case where the form of the distribution \mathcal{P} of θ is not given, we usually approximate \mathcal{P} using various functional forms. Three approaches are popular in the literature

1. Approximating \mathcal{P} by a known distribution with tunable parameters. For example, Gaussian-mixture distributions are used in variational inference for approximating the unknown distribution \mathcal{P} [4]. Consequently, the problem is reduced to estimating the covariances Σ and the means μ of the mixed Gaussian distributions. The surrogate mathematical model can be formulated as

$$x = F(w, \tilde{\theta}(\Sigma, \mu)) \quad (6)$$

where $\tilde{\theta}(\Sigma, \mu)$ is the Gaussian-mixture distribution and is used to approximate θ . Even though w is known, the log probability $p(x | \Sigma, \mu)$ is usually analytically intractable due to the complicated nature of F , and therefore presents a major challenge for maximum likelihood methods for estimating Σ, μ .

2. Bayes inference method [5]. In this approach, we update our estimation of θ according given each new observation x_i to Bayes rule

$$p(\theta | x_i) = \frac{p(x_i | \theta)p(\theta)}{p(x_i)} \quad (7)$$

The Bayes inference method requires us to specify a prior $p(\theta)$, which can be difficult in the absence of a physical basis or a plausible scientific model; besides, it also requires calculating $p(x_i|\theta)$, which can be difficult to compute numerically.

3. Markov Chain Monte Carlo (MCMC). MCMC can create samples from \mathcal{P} by constructing a Markov chain. It is a sample-based method and notoriously slow to converge, and sometimes suffers from non-convergence [6].

Method	Requires Sampling	Requires Log Likelihood	Has Explicit Loss Functions	Parametrizes \mathcal{P}
Gaussian-Mixture Approximation	✗	✓	✓	✓
Bayes Inference	✗	✓	✓	✗
MCMC	✓	✗	✗	✗
ANA	✓	✗	✓	✓

Table 2: Comparison of ANA and traditional methods.

Our approach, adversarial numerical analysis (ANA), is based on minimizing the discrepancy between the actual random process $x = F(w, \theta)$ and estimated random process $\tilde{x} = F(w, \tilde{\theta})$. Here $\tilde{\theta}$ is our current estimation for the true parameter θ and is updated as the minimization proceeds. The key is that we can formulate the discrepancy between statistical properties of x and \tilde{x} (called discriminator loss) with a neural network. The idea is borrowed from generative neural nets (GAN), where a neural network D_ξ , parametrized by ξ , tries to discriminate actual random variable x and the estimated random variable \tilde{x} . Meanwhile, we update $\tilde{\theta}$ to generate samples \tilde{x} that are indistinguishable from x . By updating the neural network and $\tilde{\theta}$ simultaneously, at equilibrium, we obtain a $\tilde{\theta}$ such that the neural network cannot discriminate x and \tilde{x} , even though we keep updating ξ to reinforce the neural network’s discrimination ability. This indicates that the distribution \tilde{x} is indistinguishable from x , under the probability metric determined by the neural network.

How can the discriminator neural network measure the discrepancy between two probability distributions? The answer is that the choice of the loss functions $L^D(x, \tilde{x}; \xi)$ for updating ξ (assuming $\tilde{\theta}$ is fixed), and the loss functions $L^F(\tilde{x}) = L^F(F(w, \tilde{\theta}))$ for updating $\tilde{\theta}$ (assuming ξ is fixed) together determines the probability metric. For example, by properly choosing L^D and L^F (see Eq. (18) for such an example), we actually obtain the maximum likelihood estimator for θ (if θ is subject to a Dirac delta distribution) at equilibrium and the corresponding probability distance metric is Kullback-Leibler divergence. Even though we have not formulated it explicitly; more importantly, we do not have to compute log likelihood function analytically. It has been realized that some of the loss functions in GANs result in optimal estimators for specific probabilistic metrics for D . For example,

- Vanilla GANs correspond to the Jensen-Shannon divergence.
- Wasserstein GANs to the Wasserstein distance.

- Kullback-Leibler GANs to the KL divergence.

To approximate the unknown distribution \mathcal{P} of θ , we can parametrize the probability distribution with certain function forms. In the case when \mathcal{P} is **low-dimensional**, conventional functional forms such as linear basis functions, radial basis functions, and polynomial basis functions can be used to approximate the density function \mathcal{P} . In this case, the problem is reduced to estimating some coefficients.

However, when \mathcal{P} is a **high-dimensional** multi-variate distribution, those methods can be too computationally expensive. It has been found that neural networks are very good candidates to transform simple distributions to very complex ones. In GAN applications, such neural networks are called *generative neural networks*. We adopt this approach in ANA and use a neural network $D_\xi : \mathbb{R}^d \rightarrow \mathbb{R}^d$ to represent d -dimensional unknown distributions \mathcal{P} (d' and d are not necessarily equal). The generative neural net $G_\eta : \mathbb{R}^{d'} \rightarrow \mathbb{R}^d$ transforms a random variable u whose distribution is easy to sample from, e.g., a multivariate Gaussian distribution $\mathcal{N}(0, I_d)$, to another random variable $G_\eta(u)$. We approximate θ with $G_\eta(u)$ by tuning the parameters η . Figure 1 illustrates the model formulation of ANA and Table 2 compares the difference between ANA and traditional approaches.

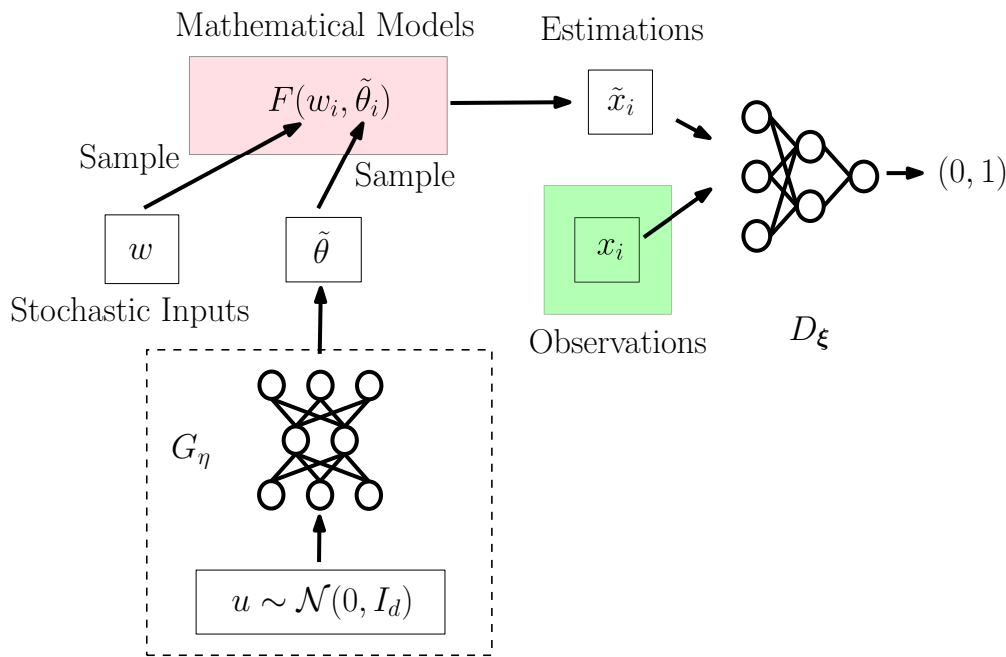


Figure 1: Graphical illustration of adversarial numerical analysis. $\{x_i\}$ are observations, $w_i, \tilde{\theta}_i$ are realizations of w and $\tilde{\theta}$ respectively ($\tilde{\theta} = G_\eta(u)$ is an approximation to the true random variable θ). D_ξ is the discriminator. We parametrize \mathcal{P} with a neural network G_η and the problem is reduced to estimating η (the dashed block). With estimated η , $G_\eta(u)$ is our approximation to the unknown random variable θ . When \mathcal{P} is a Dirac Delta distribution, the dashed block is not needed.

Now we discuss how ANA can be implemented. The idea is adversarial training, where we simultaneously (1) update $\tilde{\theta}$ such that the discriminator D_ξ cannot distinguish x and \tilde{x} ; (2) update ξ so such the discriminator is better at distinguishing x and \tilde{x} . At equilibrium,

the generated outputs \tilde{x} will be indistinguishable from real random processes x in the sense of small probability discrepancy, determined by L^D and L^F . To be more concrete, assume that we have multiple observations $\{x_i\}$, the algorithm works as follows

1. Generate realizations of w : $w_i, i = 1, 2, \dots, N$.
2. Generate realizations of $u \sim \mathcal{N}(0, I_d)$: $u_i, i = 1, 2, \dots, N$.
3. Compute $\tilde{x}_i = F(w_i, G_\eta(u_i))$.
4. Compute the discrepancy between predictions $\{\tilde{x}_i\}$ and observations $\{x_i\}$ in terms of probability distribution metrics: $d = L^D(\{x_i\}, \{\tilde{x}_i\}; \xi), i = 1, 2, \dots, N$.
5. If d is smaller than a predetermined threshold, stop and $G_\eta(u)$ is the approximation to θ ; otherwise, update η according to the gradient

$$\nabla_\eta L^F(\{F(w_i, G_\eta(u_i))\}_i) \quad (8)$$

and repeat Step 1–4.

Note we have abused the notation L^D, L^F for both random variables/processes and discrete samples. The discrete version can be viewed as the numerical approximation to the random variables/processes counterparts. The explicit expression is given in Section 2.2.

For our code implementation, we use automatic differentiation [7] for computing Eq. (8). This is key for implementing these methods quickly even for complex models. The model F can be rather complicated: it can be a one-step simulation in the stochastic process, or a partial differential equation solver, or a sequence of coupled numerical procedures. For this purpose, we developed ADCME¹, a `Julia` package, with `TensorFlow` and `PyTorch` backends, specially designed for engineering applications with automatic differentiation and parallel computing capabilities. It provides mathematically friendly syntax and supports hybrid programming with `C/C++` and `Julia`. It has the built-in optimizers and loss functions mentioned above. Those favorable features make it suitable for conducting adversarial numerical analysis for inverse modeling.

In the numerical examples, we first show that the method can calibrate an unknown parameter (a Dirac Delta distribution), and at the same time learn an unknown distribution. Then we demonstrate that the proposed algorithm is very effective in learning different complicated distributions, with the same neural network architectures for D_ξ and G_η respectively, for hidden physical parameters within a partial differential equation system. Next, we benchmark different optimizers for ANA. We demonstrate numerically that the popular optimizer in engineering—`LBFGS`—perform equally well or even better in some cases compared to stochastic gradient descent optimizers. It converges faster and more smoothly than `ADAM` and `RMSPprop`. We also discuss present numerical evidence for the convergence of the algorithm, which is consistent with our theoretical analysis. Throughout the numerical examples, we do not find significant differences in performance between the different loss functions.

¹Available at <https://github.com/kailaix/ADCME.jl>

This paper is organized as follows: in Section 2 we introduce adversarial numerical analysis, and propose an optimization algorithm for the framework. In Section 3 we analyze the convergence of ANA based on Kullback-Leibler divergence, a special case of ANA for application in parameter calibration of CIR processes. In Section 4, extensive numerical experiments are carried out, which include applications in uncertainty quantification, parameter inference, and option pricing. The numerical experiments also demonstrate our analysis in Section 3. Finally, we conclude with a general discussion of the method in Section 5.

2. Adversarial Numerical Analysis

2.1. Adversarial Numerical Analysis Description

To illustrate the concept of adversarial numerical analysis, we consider a parameter inference problem in stochastic processes. The example is intended to be explanatory and ANA is applicable even when the closed-form density function is not available or the unknowns are probability distributions.

Consider the parameter calibration of the mean in the Cox, Ingersoll and Ross process (CIR process) [8]. The CIR process

$$dr_t = \kappa(\theta - r_t)dt + \sqrt{r_t}\sigma dW_t \quad (9)$$

is used for interest rate modeling; (κ, θ, σ) are model parameters. $\{W_t, t \geq 0\}$ is the standard Brownian motion; the interest rate r_t moves in the direction of its mean θ at speed κ , $r_t\sigma^2$ is the diffusion function. Assume we are given a sample path $\mathbf{R} = \{R_1, R_2, \dots, R_n\}$ with time interval Δt , and σ, κ are known. The task is to estimate the mean θ . Many methods exist for such a problem, such as maximum likelihood methods [8] and ordinary least square methods [9].

The idea of ANA is to match the distribution of simulated data and that of observed data. For this example, we define the observed data as $\{(R_i, R_{i+1})\}_{i=1}^n$. The numerical model corresponding to the continuous one Eq. (9) is the Euler Maruyama scheme

$$\tilde{y}_i = F((x_i, W_i), \theta) = \left(x_i, x_i + \kappa(\theta - x_i)\Delta t + \sigma\sqrt{x_i\Delta t}W_i \right) \quad (10)$$

with stochastic input $W_i \sim \mathcal{N}(0, 1)$ and x_i is randomly drawn from the sample path. A discriminative neural network $D_\xi : \mathbb{R}^2 \rightarrow (0, 1)$ is used to measure the discrepancy between $\{y_i\}$ and $\{\tilde{y}_i\}$. The goal of the neural network is to output 1 for y_i and 0 for \tilde{y}_i

$$D_\xi(y_i) \approx 1 \quad D_\xi(\tilde{y}_i) \approx 0 \quad (11)$$

under this assumption; one choice of the model loss function is (recall that \tilde{y}_i depends on θ)

$$L^F(\{\tilde{y}_i\}) = -\frac{1}{n} \sum_{i=1}^n \log D_\xi(\tilde{y}_i) \quad (12)$$

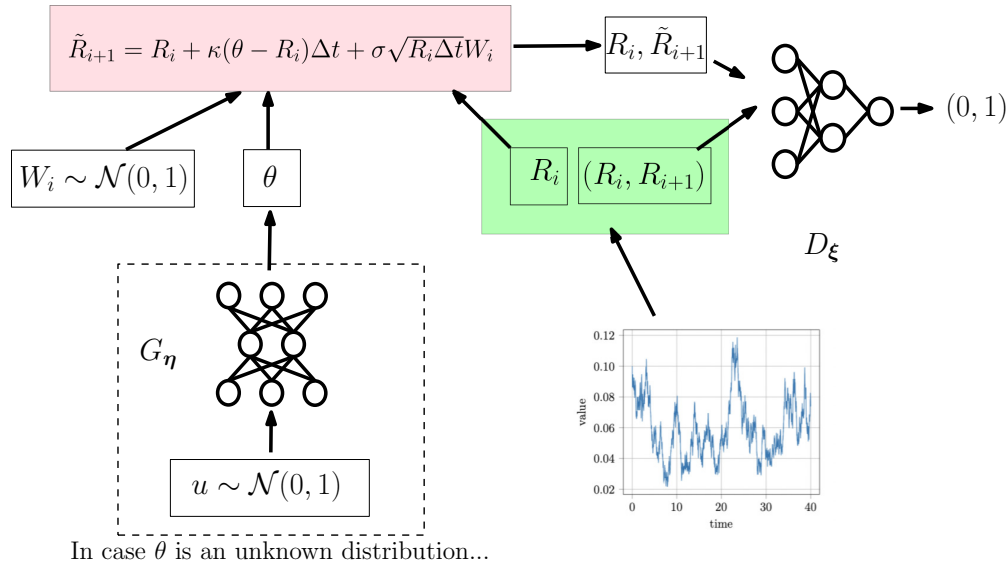


Figure 2: ANA pipeline for Eq. (9). The outputs are obtained from simulated samples \tilde{R}_{i+1} from inputs R_i . D_ξ discriminates $\{(R_i, \tilde{R}_{i+1})\}$ and $\{(R_i, R_{i+1})\}$.

when we drive $D_\xi(\tilde{y}_i)$ to 1 by minimizing L^F , and therefore making the simulated outputs \tilde{y}_i seem more similar to the observed ones.

By parametrizing \mathcal{P} with the neural network D_ξ , the mathematical model for the stochastic process is converted to

$$\tilde{y}_i = F((x_i, W_i), D_\xi(u)) \quad (13)$$

here $u \sim \mathcal{N}(0, 1)$, but it can also be other probability distributions such as uniform distributions, as long as we are able to draw samples. The optimization algorithm follows Algorithm 1. We can apply Algorithm 1 to the new model Eq. (13).

In our algorithm, we have used multiple optimizers for updating ξ and θ , such as gradient descent and LBFGS.

We remark that technically the method can also be used to estimate unknown parameters and distributions at the same time. Besides, we have not discussed the well-posedness and the conditioning of the problems yet but we will acknowledge its importance through the analysis of a model problem in Section 3.

2.2. Choice of Loss Functions for ANA

The discriminator neural network D_ξ shares similar features as that in GANs. In this subsection, we propose three sets of loss functions, which all come from different GAN algorithms.

Recall that D_ξ is the discrimination neural network, y_i and \tilde{y}_i are observed and simulated data respectively. The major difference between the following GANs is their loss functions.

- *Vanilla GAN* [10]. The output of D_ξ is a number in the range $(0, 1)$, and the loss

Algorithm 1 Optimization algorithm for ANA. The outer loop of the algorithm involves updating θ and an inner loop, where the discrimination neural network is updated for k times. For LBFGS, $k = 1$ is used.

- 1: **for** $i = 1, 2, 3, \dots$ **do**
- 2: **for** $j = 1, 2, \dots, k$ **do**
- 3: Generate n samples $\{w_1, w_2, \dots, w_n\}$ from \mathcal{Q}
- 4: Compute $\tilde{y}_i \leftarrow F(x_i, w_i; \theta)$, $i = 1, 2, \dots, n$
- 5: Update the discrimination neural network parameters ξ by the gradients

$$\nabla_{\xi} L^D(\{y_i\}, \{\tilde{y}_i\})$$

- 6: **end for**
- 7: Generate n samples $\{w_1, w_2, \dots, w_n\}$ from \mathcal{Q}
- 8: Compute $\tilde{y}_i \leftarrow F(x_i, bw_i; \theta)$, $i = 1, 2, \dots, n$
- 9: Compute the gradients of L^F using adjoint state methods (or automatic differentiation)

$$\mathbf{g} = \nabla_{\theta} L^F(\{\tilde{y}_i\})$$

- 10: Update θ with \mathbf{g}
 - 11: **end for**
-

functions are

$$L^F(\{\tilde{y}_i\}) = -\frac{1}{n} \sum_{i=1}^n \log D_{\xi}(\tilde{y}_i) \quad (14)$$

$$L^D(\{y_i\}, \{\tilde{y}_i\}; \xi) = -\frac{1}{n} \sum_{i=1}^n (\log(D_{\xi}(y_i)) + \log(1 - D_{\xi}(\tilde{y}_i))) \quad (15)$$

At equilibrium, $L^F = \log 2$, $L^D = \log 4$.

- *Wasserstein GAN* [11]. The last layer of the discrimination network is usually a linear layer, and the loss functions are

$$L^F(\{\tilde{y}_i\}) = \frac{1}{n} \sum_{i=1}^n D_{\xi}(\tilde{y}_i) \quad (16)$$

$$L^D(\{y_i\}, \{\tilde{y}_i\}; \xi) = -\frac{1}{n} \sum_{i=1}^n D_{\xi}(y_i) \quad (17)$$

The discrimination neural network D_{ξ} is usually restricted to those whose norm of weights are within $[-c, c]$, $c > 0$. The norm of the weights in D_{ξ} are usually restricted to $[-c, c]$, $c > 0$, so that D_{ξ} belongs to the class of Lipschitz functions. In this case,

the output of the neural network is not necessarily $(0, 1)$. At equilibrium, $L^F = 0$, $L^D = 0$.

- *Kullback–Leibler (KL) GAN* [12]. The output of D_ξ is a number in the range $(0, 1)$, and the loss functions are

$$\begin{aligned} L^F(\{\tilde{y}_i\}) &= \frac{1}{n} \sum_{i=1}^n \log \frac{(1 - D_\xi(\tilde{y}_i))}{D_\xi(\tilde{y}_i)} \\ L^D(\{y_i\}, \{\tilde{y}_i\}; \xi) &= -\frac{1}{n} \sum_{i=1}^n (\log D_\xi(\tilde{y}_i) + \log(1 - D_\xi(y_i))) \end{aligned} \quad (18)$$

At equilibrium, $L^F = 0$, $L^D = \log 4$.

Other variations of loss functions exist. A comprehensive comparison of the loss functions is out of scope but we refer readers to [12] for an excellent discussion.

The choice of optimizers is another concern for training in ANA. We attempt to compare the LBFGS optimizer, which is extensively used in engineering, with other popular optimizers in machine learning. In our experiment, we mainly use three kinds of optimizers

- **ADAM** [13]. Adam is an algorithm for first-order optimization of stochastic objective functions based on adaptive estimates of lower-order moments. We apply 5 updates to θ and 1 update to D_ξ in each iteration.
- **RMSProp** [14]. RMSProp divides the gradient by a running average of its recent magnitude. Usually it divides the learning rate by an exponentially decaying average of squared gradients. We apply 5 updates to θ and 1 update to D_ξ in each iteration.
- **LBFGS** [15]. The limited Broyden–Fletcher–Goldfarb–Shanno algorithm is a powerful approach for finding a local minimum of a nonconvex objective function. The LBFGS approximates the Hessian based on the most recent gradients. In our examples, LBFGS is used for optimizing L^F and one ADAM update is applied to D_ξ in each iteration.

3. Convergence Analysis

3.1. KL GAN Produces Maximum Likelihood Estimators

Thanks to the connection of ANA with GANs discussed in Section 1, many convergence analysis results for GANs are also applicable to ANA. There are many variants of GANs. From the perspective of divergence minimization [16], variants are proposed to minimize Kullback-Leibler distance (KL), the Jensen-Shannon distance, or the Wasserstein distance. For example, the vanilla GAN proposed in [10] is equivalent to minimizing the cross-entropy [17]. One particularly interesting case is minimizing the KL-divergence. It was shown [17] that it is equivalent to maximizing the log-likelihood function

$$\arg \min_{\eta} D_{KL}(\{x_i\}_{i=1}^n || F(w, G_\eta(u))) = \arg \max_{\eta} \log \sum_{i=1}^n l_\eta(x_i) \quad (19)$$

where $l_\eta(x)$ is the log likelihood function and $\{x_i\}_{i=1}^n$ is the discrete distribution of the observations x . The optimal η is exactly the maximum likelihood estimator. [10] showed that using eq. (18) is equivalent to minimizing eq. (22) in expectation, under the assumption that the discrimination neural network is optimal.

It is known that under some regularity conditions on the family of distributions, the maximum likelihood estimator $\hat{\eta}_n$ is consistent, i.e., if η^* is the true parameter, we have $\hat{\eta}_n \rightarrow \eta^*$, $n \rightarrow \infty$ [18]. In addition, we have the asymptotic normality for maximum likelihood estimator [19]

$$\sqrt{n}(\hat{\eta}_n - \eta^*) \rightarrow \mathcal{N}\left(0, \frac{1}{I(\eta^*)}\right) \quad (20)$$

where $I(\eta)$ is the Fisher information

$$I(\eta) = -\mathbb{E}_{x \sim \mathcal{U}_x} \left(\frac{\partial^2}{\partial \eta^2} \log l_\eta(x) \right) \quad (21)$$

Remark 1. *The discussion above holds true if θ is subject to a Dirac delta distribution. In this case, the minimization problem becomes*

$$\arg \min_{\theta} D_{KL}(\{x_i\}_{i=1}^n || F(w, \theta)) = \arg \max_{\theta} \log \sum_{i=1}^n l_\theta(x_i) \quad (22)$$

and let the maximum likelihood estimator for n samples be $\hat{\theta}_n$, and the exact parameter is θ^* , then we have

$$\sqrt{n}(\hat{\theta}_n - \theta^*) \rightarrow \mathcal{N}\left(0, \frac{1}{I(\theta^*)}\right) \quad (23)$$

3.2. Theoretical Analysis for the CIR Example with KL Divergence

In this section, we analyze the convergence of ANA for estimating θ and κ in Eq. (9). The analysis for other parameters is similar. The analysis also gives us some insights into when the mathematical problem is proposed and thus guides the design of algorithms.

In the last section Section 3.1 we showed that if we use KL GAN, under the assumption that the discrimination neural network is optimal, κ , θ will converge to the maximum likelihood estimator in expectation. We assume that all those assumptions are satisfied, and therefore we can focus on analyzing the convergence of the maximum likelihood estimators for θ and κ . Note the choice of KL GAN is merely for analysis purposes and reconstructing the maximum likelihood estimator from ANA is not the final goal. But since the maximum likelihood estimator is well studied the analysis based on this particular choice helps us understand the theoretical aspect of ANA better.

3.2.1. Convergence for the τ estimator

We revisit the CIR example in Section 2.1. Recall in the CIR example, $y = F(w, \theta)$, samples of the known stochastic process w have the form $W_i \sim \mathcal{N}(0, 1)$ and the output (x_i, y_i) are two consecutive sample with time interval Δt . x_i and y_i are related by

$$y_i = x_i + \kappa(\tau - x_i)\Delta t + \sigma\sqrt{x_i\Delta t}W_i \quad (24)$$

The probability density function of y_i given the observation x_i is given by

$$p(y|x) = \frac{1}{\sqrt{2\pi\sigma^2x\Delta t}} \exp\left(-\frac{1}{2}\left(\frac{y-x-\kappa(\tau-x)\Delta t}{\sigma\sqrt{x\Delta t}}\right)^2\right) \quad (25)$$

Assuming that x has the probability density function $f(x)$, then the log likelihood function for the joint distribution (x, y) is

$$l_\tau(x, y) = -\frac{1}{2}\left(\frac{y-x-\kappa(\tau-x)\Delta t}{\sigma\sqrt{x\Delta t}}\right)^2 + \log f(x) - \log(\sigma\sqrt{2\pi x\Delta t}) \quad (26)$$

Therefore, assume we have observations (x_i, y_i) , $i = 1, 2, \dots, n$, which are consecutive samples with time interval Δt , the empirical log likelihood function is

$$\sum_{i=1}^n l_\tau(x_i, y_i) = -\frac{1}{2}\sum_{i=1}^n \left(\frac{y_i - x_i - \kappa(\tau - x_i)\Delta t}{\sigma\sqrt{x_i\Delta t}}\right)^2 + \sum_{i=1}^n \log f(x_i) - \sum_{i=1}^n \log(\sigma\sqrt{2\pi x_i\Delta t}) \quad (27)$$

the maximum likelihood estimator can be computed

$$\sum_{i=1}^n l'_\tau(x_i, y_i) = 0 \Rightarrow \hat{\tau}_n = \frac{\frac{1}{n}\sum_{i=1}^n \frac{y_i}{x_i} + \kappa\Delta t - 1}{\left(\frac{1}{n}\sum_{i=1}^n \frac{1}{x_i}\right)\kappa\Delta t} \quad (28)$$

According to the discussion, if we use KL divergence as the discrepancy measure of the real sample-path and generated ones, $\hat{\tau}$ at the Nash equilibrium will converge to $\hat{\tau}_n$ under mild assumptions. Let τ^* be the exact solution, we prove that as $\Delta t \rightarrow 0$, $n \rightarrow \infty$, $\hat{\tau}_n \rightarrow \tau^*$. We always assume convergence in the distribution for probability convergence.

Theorem 1. Assume that $\mathbb{E}\left(\frac{1}{x}\right) = X_{-1} \in (0, \infty)$, for sufficiently small $|\Delta t|$, we have

$$\hat{\tau}_n \rightarrow \tau^* + \mathcal{O}(\Delta t) \quad n \rightarrow \infty \quad (29)$$

in addition, the corresponding Fisher information

$$I(\tau) = \frac{\kappa^2\Delta t X_{-1}}{\sigma^2} \quad (30)$$

and consequently

$$\sqrt{n}(\hat{\tau}_n - \tau^*) \rightarrow \mathcal{N}\left(0, \frac{\kappa^2\Delta t}{\sigma^2 X_{-1}}\right) \quad (31)$$

Proof. Since $\mathbb{E}\left(\frac{1}{x}\right) < \infty$, by law of large numbers we have

$$\frac{1}{n}\sum_{i=1}^n \frac{1}{x_i} \rightarrow X_{-1} \quad n \rightarrow \infty \quad (32)$$

We first verify that $\mathbb{E}\left(\frac{y}{x}\right) < \infty$ so that the law of large numbers hold. For CIR processes, we have [20]

$$\mathbb{E}[y|x] = xe^{-\kappa\Delta t} + \tau^*(1 - e^{-\kappa\Delta t}) \quad (33)$$

thus

$$\mathbb{E}\left[\frac{y}{x}\right] = \mathbb{E}\left[\mathbb{E}\left[\frac{y}{x}\middle|x\right]\right] = e^{-\kappa\Delta t} + \tau^*(1 - e^{-\kappa\Delta t})X_{-1} < \infty \quad (34)$$

therefore

$$\frac{1}{n} \sum_{i=1}^n \frac{y_i}{x_i} \rightarrow e^{-\kappa\Delta t} + \tau^*(1 - e^{-\kappa\Delta t})X_{-1} \quad n \rightarrow \infty \quad (35)$$

Plug eqns. (32) and (35) into eq. (28) we obtained using the continuous mapping theorem [21]

$$\hat{\tau}_n \rightarrow \frac{\tau^*(1 - e^{-\kappa\Delta t})}{\kappa\Delta t} + \frac{e^{-\kappa\Delta t} + \kappa\Delta t - 1}{X_{-1}\kappa\Delta t} = \tau^* + \mathcal{O}(\Delta t)$$

□

Remark 2. The constraint $\mathbb{E}\left(\frac{1}{x}\right) = X_{-1} < \infty$ is satisfied asymptotically. Assume $2\kappa\tau > \sigma^2$, and n is large enough so x_i is subject to the asymptotic distribution of the CIR process, which is a gamma distribution with density function

$$h(r) = \frac{w^\nu}{\Gamma(\nu)} r^{\nu-1} e^{-wr}, \quad w = \frac{2\kappa}{\sigma^2}, \quad \nu = \frac{2\kappa\tau^*}{\sigma^2} \quad (36)$$

thus we have

$$\mathbb{E}\left(\frac{1}{x}\right) = \int_0^\infty \frac{1}{r} h(r) dr = \frac{1}{\tau^*} < \infty \quad (37)$$

If x is sampled from the asymptotic distribution (when n is very large), the Fisher information is

$$I(\tau) = \frac{\kappa^2\Delta t}{\sigma^2\tau^*} \quad (38)$$

therefore we have

$$\sqrt{n}(\hat{\tau}_n - \tau^*) \rightarrow \mathcal{N}\left(0, \frac{\sigma^2\tau^*}{\kappa^2\Delta t}\right) \quad (39)$$

The condition eq. (29) and eq. (39) indicates that for $\hat{\tau}_n \rightarrow \tau^*$ as $\Delta t \rightarrow 0$, $n \rightarrow \infty$, the following condition is sufficient

$$n\Delta t \rightarrow \infty, \quad \Delta t \rightarrow 0 \quad (40)$$

for example, we let $\Delta t = \frac{1}{\sqrt{n}}$, i.e., $n = \frac{1}{\Delta t^2}$, then the condition eq. (40) is satisfied.

3.2.2. Convergence for the κ estimator

We assume that τ and σ are known and we want to estimate κ , whose true value is κ^* .

Theorem 2. Assume that $\mathbb{E}(x) = X_0 \in (0, \infty)$, $\mathbb{E}\left(\frac{1}{x}\right) = X_{-1} < \infty$, for sufficiently small $|\Delta t|$, we have

$$\hat{\kappa}_n \rightarrow \kappa^* + \mathcal{O}(\Delta t) \quad n \rightarrow \infty \quad (41)$$

in addition, the corresponding Fisher information

$$I(\kappa) = \frac{\Delta t}{\sigma^2}(\tau^2 X_{-1} - 2\tau + X_0) \quad (42)$$

and consequently

$$\sqrt{n}(\hat{\kappa}_n - \kappa^*) \rightarrow \mathcal{N}\left(0, \frac{\sigma^2}{\Delta t(\tau^2 X_{-1} - 2\tau + X_0)}\right) \quad n \rightarrow \infty \quad (43)$$

Proof. The log-likelihood function for estimating κ is

$$l_\kappa(x, y) = -\frac{1}{2} \left(\frac{y - x - \kappa(\tau - x)\Delta t}{\sigma\sqrt{x\Delta t}} \right)^2 + \log f_1(x) - \log(\sigma\sqrt{2\pi x\Delta t}) \quad (44)$$

and therefore the empirical log likelihood function is

$$\sum_{i=1}^n l_\kappa(x_i, y_i) = -\frac{1}{2} \sum_{i=1}^n \left(\frac{y_i - x_i - \kappa(\tau - x_i)\Delta t}{\sigma\sqrt{x_i\Delta t}} \right)^2 + \sum_{i=1}^n \log f_1(x_i) - \sum_{i=1}^n \log(\sigma\sqrt{2\pi x_i\Delta t}) \quad (45)$$

the maximum likelihood estimator can be computed

$$\sum_{i=1}^n l'_\kappa(x_i, y_i) = 0 \Rightarrow \hat{\kappa}_n = \frac{1}{\Delta t} \frac{\tau \frac{1}{n} \sum_{i=1}^n \frac{y_i}{x_i} - \frac{1}{n} \sum_{i=1}^n y_i - \tau + \frac{1}{n} \sum_{i=1}^n x_i}{\tau^2 \frac{1}{n} \sum_{i=1}^n \frac{1}{x_i} - 2\tau + \frac{1}{n} \sum_{i=1}^n x_i} \quad (46)$$

By the law of large numbers we have

$$\frac{1}{n} \sum_{i=1}^n \frac{1}{x_i} \rightarrow X_{-1} \quad \frac{1}{n} \sum_{i=1}^n x_i \rightarrow X_0 \quad (47)$$

in addition, we have

$$\frac{1}{n} \sum_{i=1}^n y_i \rightarrow \mathbb{E}[\mathbb{E}[y|x]] = X_0 e^{-\kappa^* \Delta t} + \tau(1 - e^{-\kappa^* \Delta t}) \quad (48)$$

Plug eqns. (47) and (48) into eq. (46) and note $e^{-\kappa^* \Delta t} \rightarrow 1 - \kappa^* \Delta t$, $\Delta t \rightarrow 0$, we have

$$\hat{\kappa}_n \rightarrow \frac{1}{\Delta t} \frac{\tau (e^{-\kappa^* \Delta t} + \tau(1 - e^{-\kappa^* \Delta t})X_{-1}) - (X_0 e^{-\kappa^* \Delta t} + \tau(1 - e^{-\kappa^* \Delta t})) - \tau + X_0}{\tau^2 X_{-1} - 2\tau + X_0} \quad (49)$$

$$\rightarrow \kappa^* + \mathcal{O}(\Delta t) \quad \Delta t \rightarrow 0 \quad (50)$$

Since

$$l''_{\kappa}(x) = -\frac{(\tau - x)^2 \Delta t}{\sigma^2 x} \quad (51)$$

we have

$$I(\kappa) = -\mathbb{E}(l''_{\kappa}(x)) = -\frac{\Delta t}{\sigma^2} \left(\tau^2 \mathbb{E} \left(\frac{1}{x} \right) - 2\tau + \mathbb{E}(x) \right) = \frac{\Delta t}{\sigma^2} (\tau^2 X_{-1} - 2\tau + X_0) \quad (52)$$

□

In the case where n is very large, $\frac{1}{n} \sum_{i=1}^n \frac{1}{x_i}$ and $\frac{1}{n} \sum_{i=1}^n x_i$ are approximately subject to the asymptotic distribution. Therefore, we have from eq. (37)

$$X_{-1} \approx \frac{1}{\tau} \quad X_0 \approx \tau \quad (53)$$

Consequently

$$I(\kappa) \approx 0 \quad (54)$$

which indicates that the estimator has infinite variance. However, as long as we resample from the observations such that the new training data satisfies $\tau^2 X_{-1} - 2\tau + X_0 \neq 0$, we will obtain convergence result for κ estimator. One such technique is given in Section 4.3.

Remark 3. *Given a parameter τ , let the family of distribution P_{τ} and P_{τ^*} be the true data distribution. The relationship between KL divergence and Fisher information can be described as follows for sufficiently small $|\tau - \tau^*|$ under mild assumptions*

$$D_{KL}(P_{\tau^*} || P_{\tau}) \approx \frac{1}{2} (\tau - \tau^*)^T I(\tau^*) (\tau - \tau^*) \quad (55)$$

thus if $I(\tau^) \approx 0$, we can see that $D_{KL}(P_{\tau^*} || P_{\tau})$ will have vanishing gradients and Hessians at $\tau = \tau^*$. This may lead to difficulty during optimization.*

4. Numerical Examples

In this section, we present four numerical examples. The mathematical models for those problems can all be formulated in the form of $x = F(w, \theta)$ and therefore ANA is applicable for those cases. The extensive numerical results also demonstrate the generality of the method.

4.1. Estimation and Uncertainty Quantification of Hidden Parameters in PDEs

In this example, the unknown parameter θ consists of an unknown distribution and an unknown parameter. The unknown distribution is parametrized by a neural network. We simultaneously estimate both the distribution and the parameter.

Consider a Poisson equation with Dirichlet boundary condition

$$\begin{cases} -\nabla \cdot (a(x) \nabla u(x)) = 1 & x \in (0, 1) \\ u(0) = u(1) = 0 & \text{otherwise} \end{cases} \quad (56)$$

October 16, 2019

where

$$a(x) = 1 - 0.9 \exp\left(-\frac{(x - \mu)^2}{2\sigma^2}\right) \quad (57)$$

Assume that μ and σ are both unknown, and there is model form uncertainty in μ , i.e., $\mu \sim \mathcal{P}$ for some unknown probability distribution \mathcal{P} . Our goal is that given many observations \mathbf{u}_i , $i = 1, 2, \dots, N$, where $\mathbf{u}_i \in \mathbb{R}^n$ are observations $u(h)$, and each u_i consists of $n = 100$ nodal values of $u(x)$, i.e., $u(2h), \dots, u(nh)$, $h = \frac{1}{n+1}$, we want to determine σ and \mathcal{P} .

Traditionally, this is usually done under the Bayesian framework where a priori information is imposed on \mathcal{P} and the transformation of probability in the forward model is calculated or approximated. However, this approach may be infeasible for complicated problems where the probabilistic relationship between data and parameter is analytically intractable, i.e., expressing $p(u(h), u(2h), \dots, u(nh) | \mu, \sigma)$ in a closed-form. We present an example where ANA can be used for solving such problems.

To parametrize \mathcal{P} , we consider a neural network $N : \mathbb{R}^d \rightarrow \mathbb{R}$, $d = 10$; the inputs of neural network are samples from the uniform distribution $\mathcal{U}([-1, 1]^d)$ while the output is a generated sample of μ . To discretize eq. (56), we consider the central difference scheme

$$\begin{aligned} -a_{i-\frac{1}{2}}u_{i-1} + (a_{i-\frac{1}{2}} + a_{i+\frac{1}{2}})u_i - a_{i+\frac{1}{2}}u_{i+1} &= h^2, & i = 1, 2, \dots, n \\ u_0 = u_{n+1} &= 0 \end{aligned} \quad (58)$$

where $a_{j \pm \frac{1}{2}} = a(h(j \pm \frac{1}{2}))$ which depends on μ and σ . The equation eq. (58) leads to a tridiagonal system and can be solved using the Thomas algorithm [22]. The computation pipeline is shown in fig. 3. The loss functions for F_θ and the discrimination neural network are chosen to be Wasserstein GAN losses. We use `RMSProp` with learning rate 10^{-4} and batch size 32. The true $\sigma^* = 0.1$ and the true distribution for μ is

$$\mu^* \sim \mathcal{N}(0.3, 0.1) \quad (59)$$

Figure 4 shows the results of ANA. In the first plot, we show the model loss and discriminator loss. We see that the discriminator loss converges to 0, implying that the discriminator has been successfully fooled. The model loss oscillates around 0. In the second plot, we see that the estimated σ converges to σ^* after around 1000 iterations. The values then oscillate around 0.1 due to the intrinsically adversarial optimization. The last plot shows the true distribution of μ^* and generated distribution for μ after iteration 38,000. We see that the generated distribution matches the true distribution reasonably well.

4.2. Uncertainty Quantification with Multimodal Distribution

We consider a variant of Section 4.1. This example demonstrates that ANA can be used to learn a rather complicated distribution such as multimodal ones.

Different from the last section, we assume that σ is known. Besides, μ is subject to a nontrivial distribution, e.g., Gaussian mixture distribution,

$$p = 0.4\mathcal{N}(0.3, 0.1) + 0.6\mathcal{N}(0.8, 0.05) \quad (60)$$

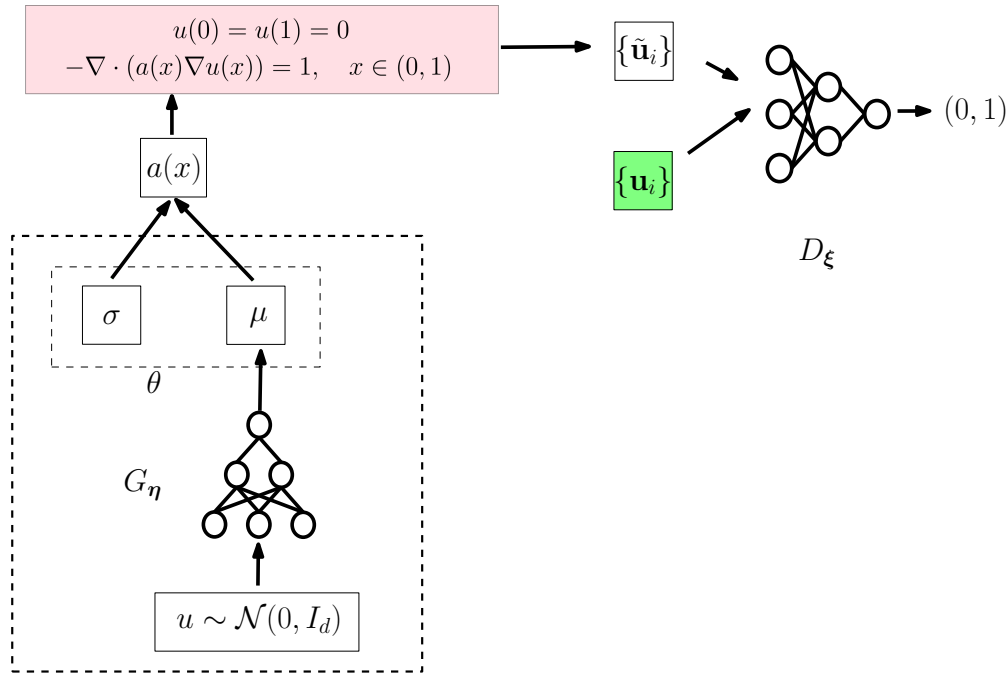


Figure 3: The ANA computation pipeline for eq. (58).

The generated samples are shown in the first plot in fig. 5. ANA is carried out with the same setting as in section 4.1. We show the loss functions and the generated distribution in fig. 5. We can see that the loss functions for F_θ and the discrimination converge to 0. The generated distribution also captures the multimodal of the distribution correctly.

Other distributions for μ are also tested with the same neural network architecture and optimizer. The results in Figure 6 demonstrate that the proposed method is effective and generic in estimating the unknown distributions in the PDE system. The test distributions include

1. the Exponential distribution with a rate 1;
2. the F distribution with degrees of freedom (5, 2);
3. the Arcsine distribution in $[0, 1]$;
4. the Beta distribution with shape parameters (1, 3);
5. the Cauchy distribution with the location parameter $x_0 = 0$ and the scale parameter $b = 0.5$;
6. the raised Cosine distribution with parameters $\mu = 0.5, s = 0.5$.

We also consider 2D distributions. In this case, we assume that μ, σ are both random variables and they are subject to a 2D unknown distribution (σ and μ not necessarily independent). We increase the number of the output layer neurons from 1 to 2 for generating σ in the previous case and perform adversarial numerical analysis. For generating synthetic data, we draw (μ, σ) from the following random distributions

1. a 2D Gaussian distribution with mean (0, 3, 1.0) and a covariance matrix $\begin{pmatrix} 0.1 & -0.05 \\ -0.05 & 0.1 \end{pmatrix}$;

October 16, 2019

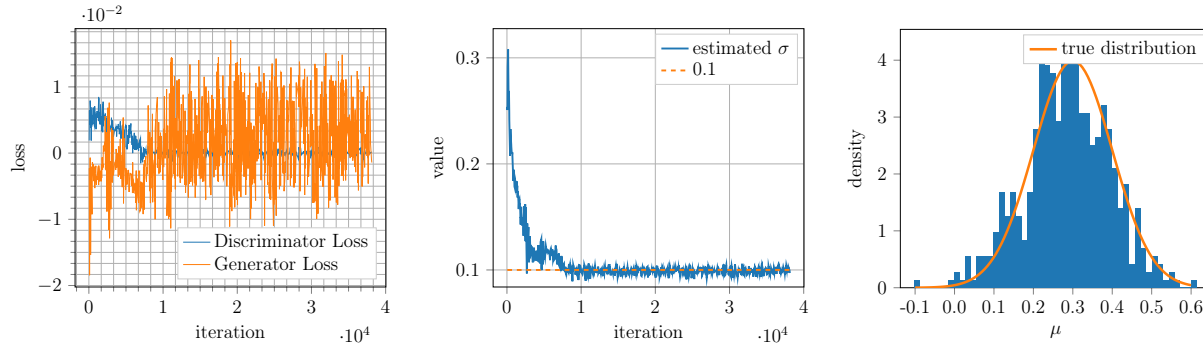


Figure 4: ANA results for eq. (58). In the first plot, we show the model loss and discriminator loss. In the second plot, we see that the estimated σ converges to σ^* after around 1000 iterations. The last plot shows the true distribution of μ^* and generated distribution for μ after iteration 38,000.

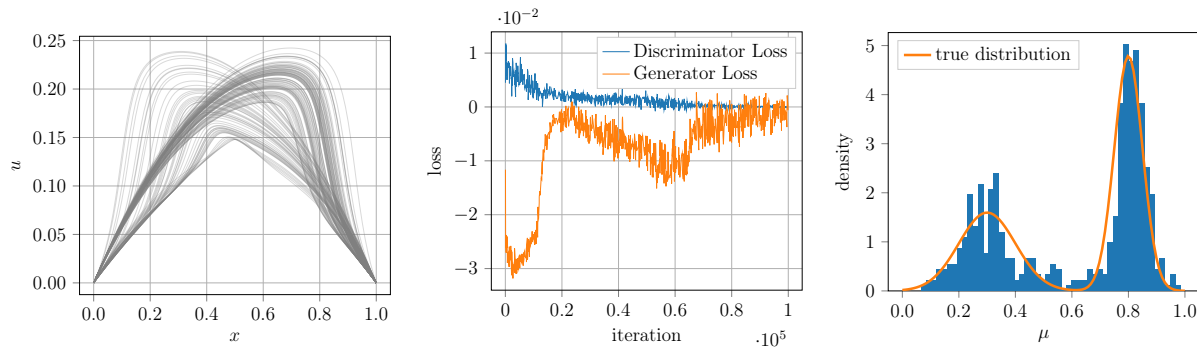


Figure 5: ANA results for eq. (58) with eq. (60). The first plot is generated samples of $u(x)$. The second plot shows the loss functions. The last plot shows the generated distribution at iteration 100,000 together with the true distribution.

2. a Dirichlet distribution with parameters $\alpha = (1.0, 1.0, 1.0)$;
3. a Dirichlet distribution with parameters $\alpha = (1.0, 2.0, 3.0)$.

since in the model σ appears as σ^2 in the coefficient function $a(x)$, we consider estimating the distribution of $(\mu, |\sigma|)$ instead of (μ, σ) . Figures 7 to 9 show the results at multiple checkpoints. It is remarkable that with the same neural network architecture and optimization scheme, ANA is able to learn a quite similar pattern as the true distribution.

4.3. Parameter Calibration for CIR Processes from Sample Paths

In this section, we consider the CIR process example considered in Sections 2.1 and 3.2 and numerically demonstrate the analysis in Section 3. We also compare different optimizers and found that LBFSGS converges most smoothly and fastest.

For better accuracy, we use the weighted Milstein scheme [23] for the simulation eq. (9)

$$y = \frac{x + \kappa(\tau - \alpha x)\Delta t + \sigma\sqrt{x}\sqrt{\Delta t}W + \frac{1}{4}\sigma^2\Delta t(W^2 - 1)}{1 + (1 - \alpha)\kappa\Delta t} \quad (61)$$

where $\alpha \in [0, 1]$ is the weight, x is the sample at last time step. In the numerical example, we let $\alpha = 0.5$, $\Delta t = 0.01$, $\sigma = 0.08$, $\kappa = 0.5$ and the exact $\tau^* = 0.06$. The length of the

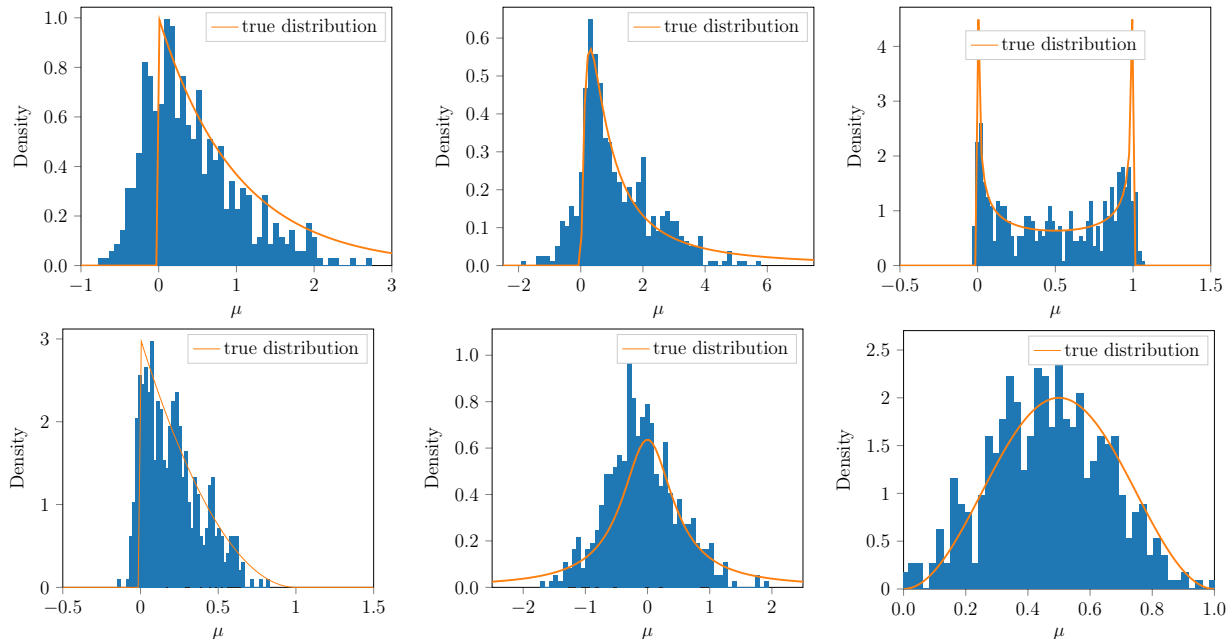


Figure 6: ANA results for estimating the probability distribution of μ where μ is subject to a different distribution for each case. The first rows are the Exponential distribution, the F distribution, and the Arcsine distribution; the second rows are the Beta distribution, the Cauchy distribution, and the raised Cosine distribution.

sample path is 4000. Figure 10 shows a realization of the sample path. The KL GAN loss functions and three optimizers (**ADAM**, **RMSProp** and **LBFSGS**) with full batch size are used.

Figure 11 shows the result of ANA. The first two plots show the generator and discrimination losses, and as we can see, they converge to 0 and $\log 4$ respectively. The third plot shows the convergence profile for τ . It is interesting to see the performance of the different optimizers. With a strong optimizer for the generator (**LBFSGS**), the convergence profile is much smoother than the others. **RMSProp** tends to produce kinks and oscillates around the true value $\tau^* = 0.06$ like **ADAM**.

Next, we discuss the convergence of κ . As indicated in Theorem 2, the convergence of κ can be very slow if $X_0 = \tau$ and $X_{-1} = \frac{1}{\tau}$, which unfortunately are true if (R_k, R_{k+1}) are sampled from a long enough sample path. This is demonstrated in fig. 12. We approximate the KL divergence with discrete KL divergence

$$L_\tau = \sum_i P_{\tau^*,i} \log \left(\frac{P_{\tau^*,i}}{P_{\tau,i}} \right) \quad L_\kappa = \sum_i P_{\kappa^*,i} \log \left(\frac{P_{\kappa^*,i}}{P_{\kappa,i}} \right) \quad (62)$$

where τ, κ are the parameters and τ^*, κ^* are their true values. $P_{\tau,i}$ is the discrete density function. In the first plot, we let $\tau = 0.06$, $\sigma = 0.08$ and vary κ . The true value is $\kappa^* = 0.5$. In the second plot, we fix $\kappa = 0.5$, $\sigma = 0.08$ and vary τ , whose true value is $\tau^* = 0.06$. We carry out the simulation eq. (61) from initial location $R_0 = 0.05$, $\Delta t = 0.001$ and path length 100,000. The result shows that near the true value, the L_κ curve is very flat, indicating small second order derivatives. Compared to L_τ , L_κ is much more oscillatory.

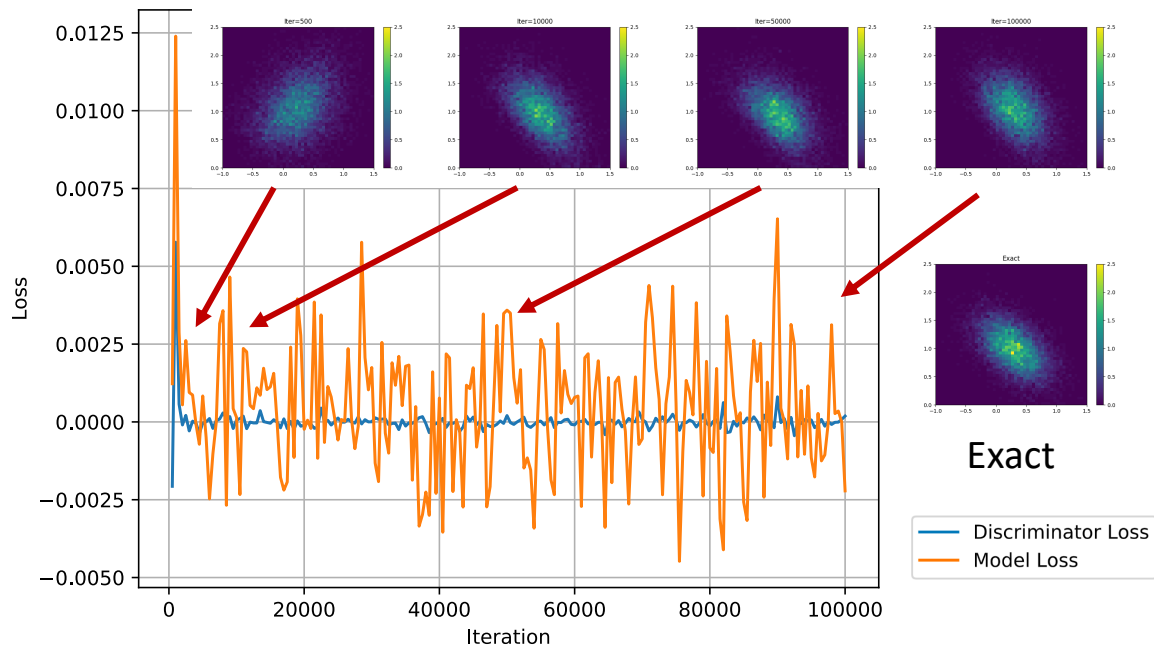


Figure 7: ANA for estimating the distribution of $(\mu, |\sigma|)$ where (μ, σ) is subject to a 2D Gaussian distribution.

A possible fix to the problem is by distorting the distribution R_k . In fig. 13-left, we artificially sample R_k from $\mathcal{U}(0.001, 0.03)$. We use $\Delta t = 0.001$, `RMSProp` with learning rate 10^{-3} for both κ and D_ξ . In each step, D_ξ is updated five times while F_θ is updated only once. We can see that the estimated κ oscillates around $\kappa^* = 0.5$ but the variance is still large. In fig. 13-right, we further consider reducing the variance by increasing n , i.e., the number of samples. Equivalently, we sample (R_k, R_{k+1}) with time interval $\Delta t = 0.1$.

4.4. Volatility Inference from Option Prices: Direct Estimation from Monte Carlo Simulation

The final example is an application of ANA to estimation volatility from European call option prices. In this case, σ is the unknown volatility parameter.

A European call option is a contract giving the holder the right to buy the underlying asset for a fixed strike price K at expiry time T . Let S_t be the price of the underlying such as the stock price at time t , then the payoff of a European call is a random variable [24]

$$P = \begin{cases} S_T - K & \text{if } S_T > K \\ 0 & \text{otherwise} \end{cases} \quad (63)$$

The stock price can be modeled as a stochastic process such as geometric Brownian motion

$$dS_t = rS_t dt + \sigma S_t dW_t \quad S_0 = s \quad (64)$$

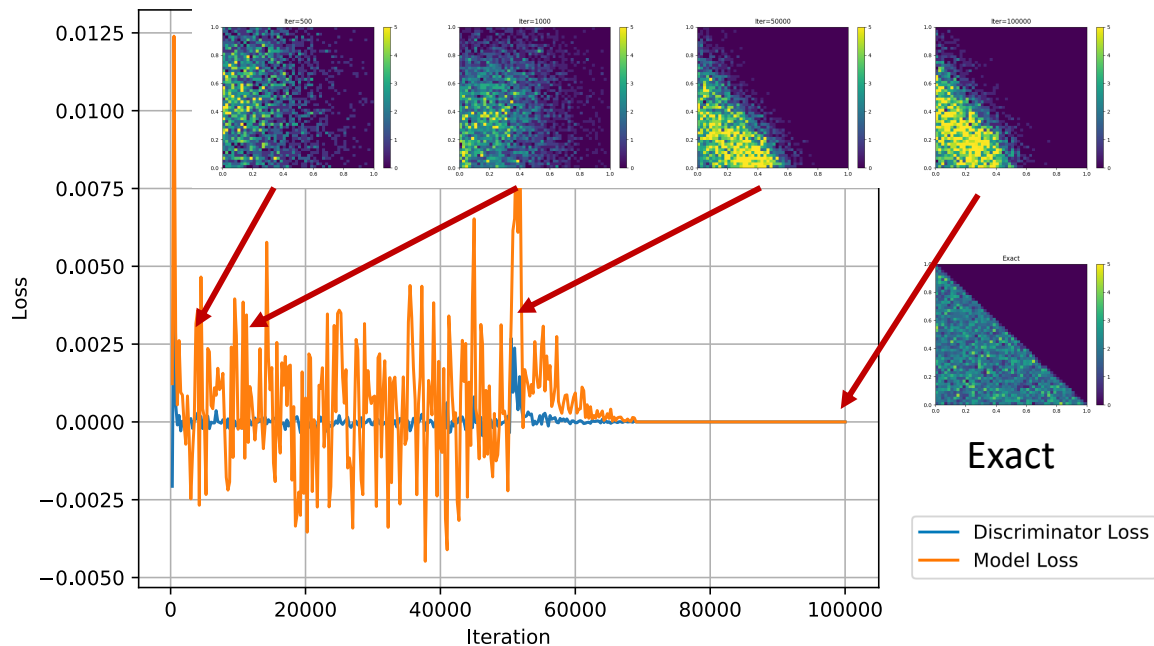


Figure 8: ANA for estimating the distribution of $(\mu, |\sigma|)$ where (μ, σ) is subject to a Dirichlet distribution with parameters $\alpha = (1.0, 1.0, 1.0)$.

where W_t is a Gaussian random variable with zero mean, σ is the volatility, μ is the expected return, and s is the spot price of the stock.

The task is to estimate σ from many observations of option prices P_i , $i = 1, 2, \dots, 100$. We consider the Monte Carlo simulation for the forward problem,

$$S_T = s \exp \left[\left(r - \frac{\sigma^2}{2} \right) T + (\sigma \sqrt{T}) W \right] \quad (65)$$

where W sampled from a standard normal distribution. Figure 15 shows samples for $s = 100$, $K = 100$, $r = 0.05$, $\sigma = 0.2$, $T = 1$.

For ANA, we use the loss functions from the vanilla GAN. RMSProp with learning rate 10^{-4} and full batch size is used. The computation pipeline is shown in fig. 14. The result is shown in fig. 16. The left plot shows the convergence of the model loss and discrimination loss. We can see that the values converge to theoretical optimal values. The right plot shows the convergence of the estimated volatility.

5. Conclusion

We have demonstrated the viability of adversarial numerical analysis for solving inverse modeling problems of the type

$$x = F(w, \theta) \quad (66)$$

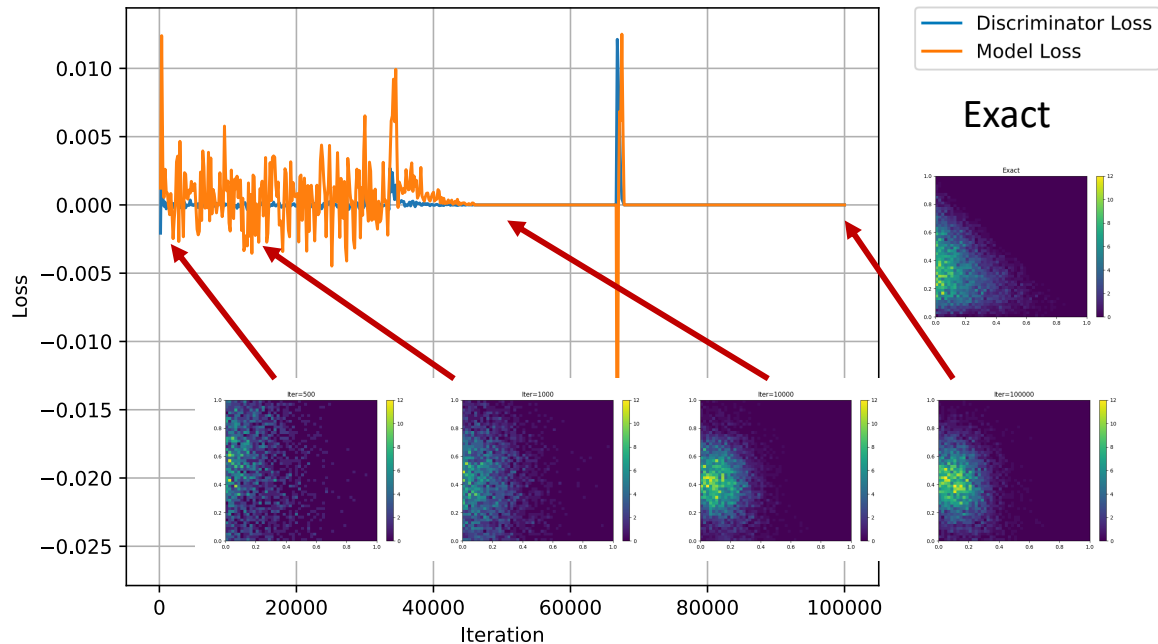


Figure 9: ANA for estimating the distribution of $(\mu, |\sigma|)$ where (μ, σ) is subject to a Dirichlet distribution with parameters $\alpha = (1.0, 2.0, 3.0)$.

where w is a known stochastic process, θ is an unknown random variable and the output x is also a random variable or process. The key ingredients for applying ANA is:

- Approximating the unknown distribution of θ by a neural network, $\tilde{\theta} = G_{\eta}(\theta)$.
- Using a discriminator neural network D_{ξ} to measure the discrepancy between the actual random process x and estimated random process $\tilde{x} = F(w, \tilde{\theta})$.
- Choosing a proper loss function for L^D and L^F .
- Adversarially training $\tilde{\theta}$ and ξ . The gradients $\frac{\partial L^D}{\partial \xi}$ and $\frac{\partial L^F}{\partial \eta}$ can be computed with automatic differentiation.

We also present a computing framework, **ADCME**, for implementing ANA. We demonstrate numerically that the approach is able to learn underlying parameters and recover complex unknown distributions. Different optimizers were benchmarked and the results showed the promising behavior of full-batch optimizers such as **LBFSGS** for engineering applications.

However, the approach also has some limitations. For example, the training of GANs can be quite expensive. To obtain the results in fig. 5, we have run 100,000 iterations, which takes up several CPU hours. Finding more efficient training algorithms, designing specialized loss functions and implementing easy-to-use high-performance toolsets is a promising line of research in the future.

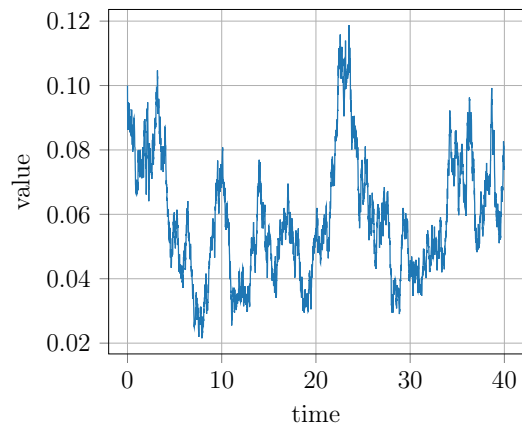


Figure 10: A sample path of the CIR process.

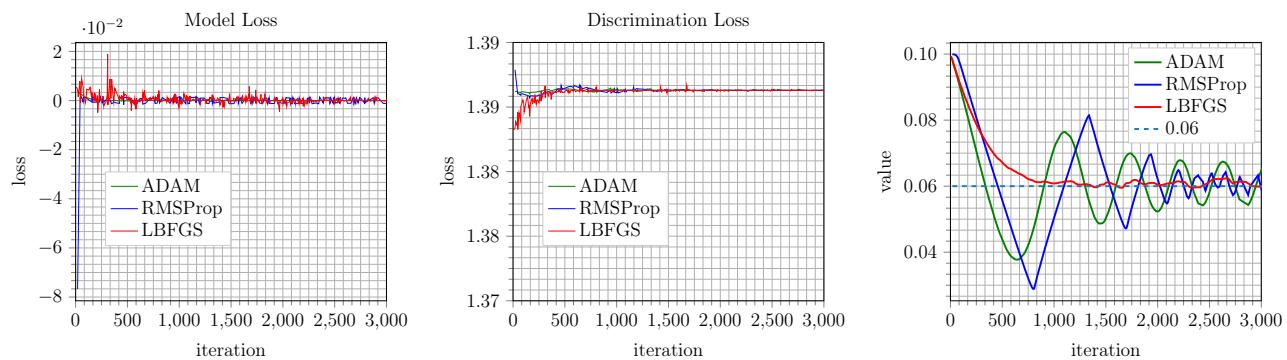


Figure 11: ANA results for eq. (61). The first two plots show the model loss and discrimination loss respectively. The third plot shows the convergence of the hidden parameter τ .

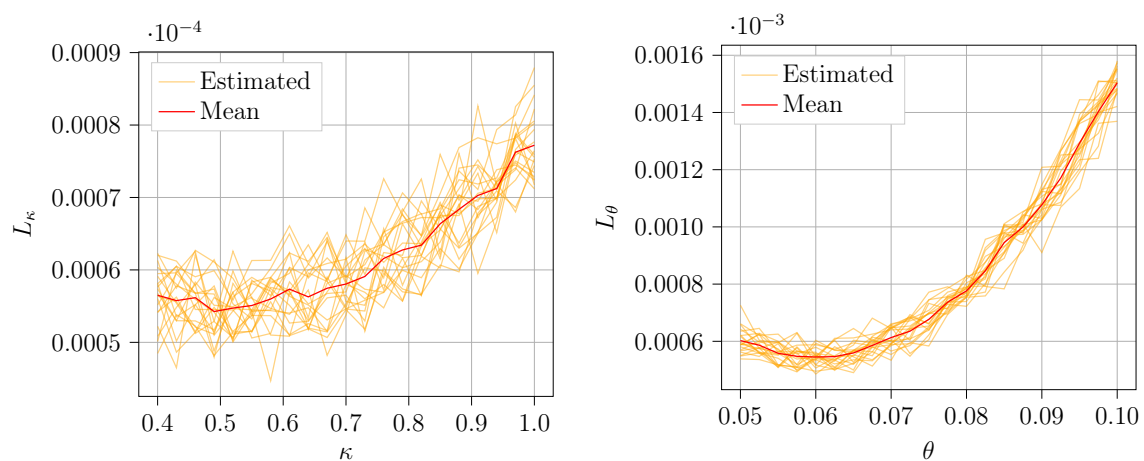


Figure 12: Discrete KL divergence as a function of κ and τ . Each plot has 10 realizations of sample paths. We see that for κ the profile is much more oscillating and the landscape at $\kappa^* = 0.5$ is nearly flat.

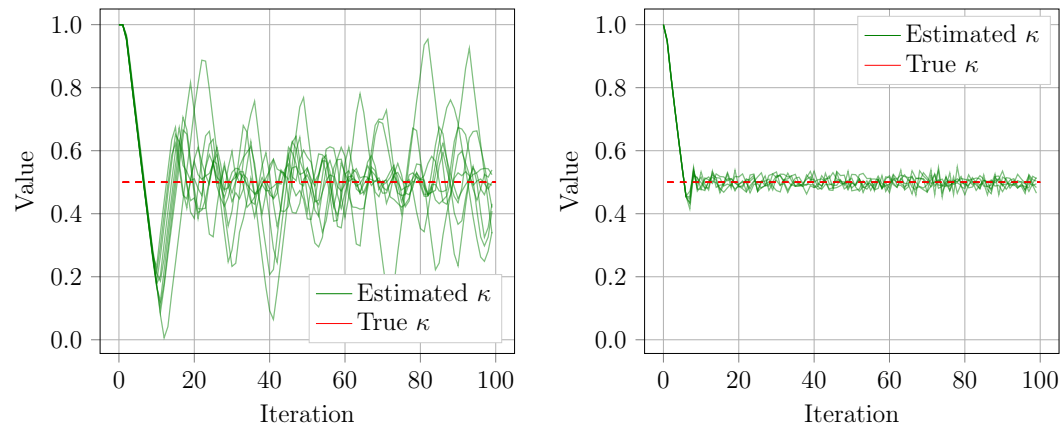


Figure 13: Convergence of κ to true value κ^* .

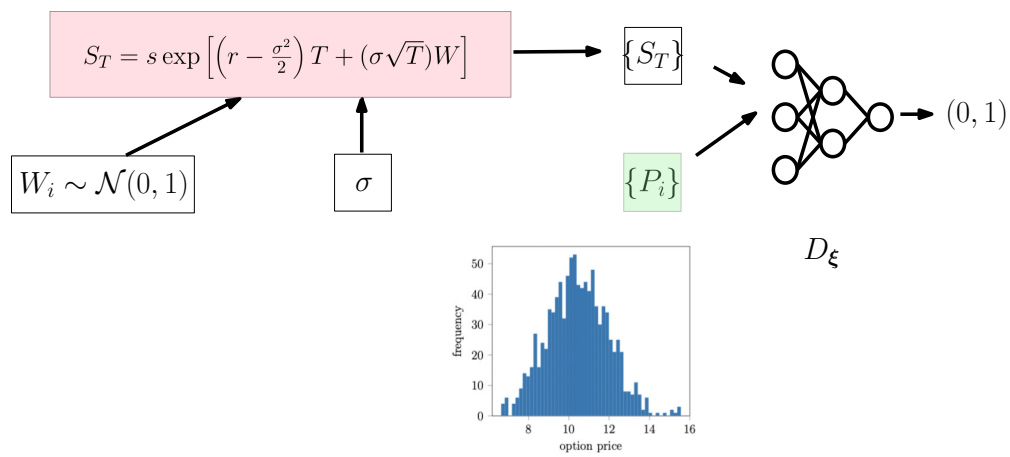


Figure 14: ANA computation pipeline for the option price example.

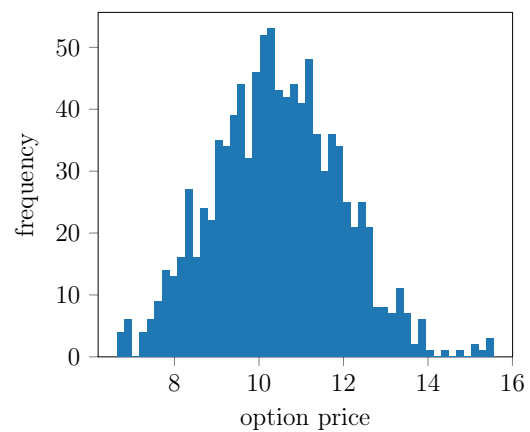


Figure 15: Observations of option prices.

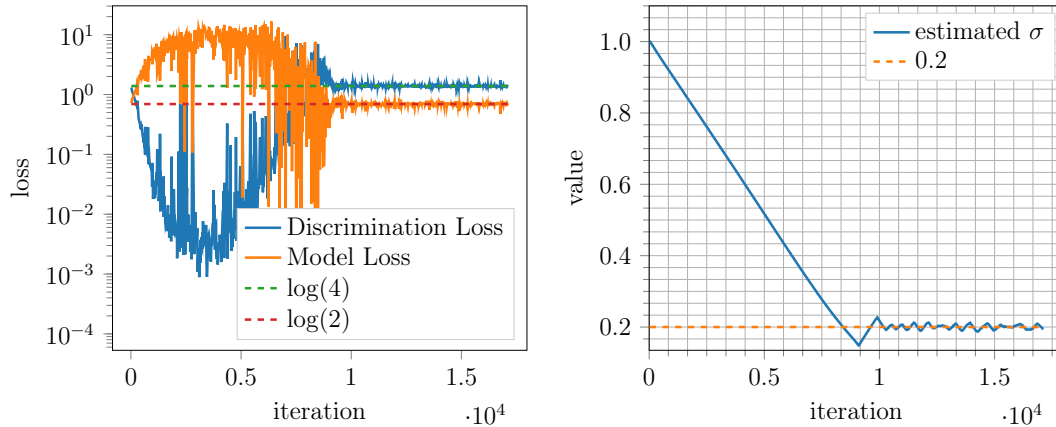


Figure 16: ANA results for the option pricing example. The first plot shows the loss function while the second shows the convergence of the hidden parameter σ .

Appendix A. Probability Metrics for ANA

Here we discuss a few probability metrics that are related to ANA; we refer the readers to [25] for more details on this topic. Note that these metrics are not mutual exclusive.

Information-theoretical Metrics [26] provide metrics for probabilities from an information-theory point of view. The idea is to find the shortest description of the data. Assume that the base of the logarithm is 2. The entropy $H(P) = \int_{\mathcal{X}} P(x) \log P(dx)$ describes the optimal average asymptotical code length for a single distribution P according to asymptotic equipartition property [27]. For two distributions P and Q for the same measurable space \mathcal{X} , assume that P is the true distribution and Q is the proposed distribution for approximating P , the relative entropy, also called Kullback-Leibler divergence, $D(P||Q) = \int_{\mathcal{X}} P(x) \log \frac{P(dx)}{Q(dx)}$ satisfies [28]

$$H(P) + D(P||Q) \leq \mathbb{E}L < H(P) + D(P||Q) + 1 \quad (\text{A.1})$$

where $\mathbb{E}L$ the expected code length for encoding P . According to eq. (A.1), if we encode P optimally, $D(P||Q)$ can be interpreted as the extra symbols we need to encode the Q . Consequently, minimizing $D(P||Q)$ reduces the redundancy in coding. The maximum likelihood method minimizes $D(P||Q)$ directly. There are many other variants for the divergence metrics. For example, the vanilla GAN proposed in [10] is equivalent to minimizing the Jensen-Shannon divergence [29]

$$d(P, Q) = \frac{1}{2}D(P||M) + \frac{1}{2}D(Q||M), M = \frac{P + Q}{2} \quad (\text{A.2})$$

The least square GAN [30] is proved to minimize the χ^2 divergence for certain parameters. There is also a class of GANs that minimizes f -divergence [12], which is also known as Ali-Silvey distances

$$d(P, Q) = \int_{\mathcal{X}} Q(x) f\left(\frac{P(dx)}{Q(dx)}\right) \quad (\text{A.3})$$

where $f : \mathbb{R}_+ \rightarrow \mathbb{R}$, $f(1) = 0$ is a convex, lower semi-continuous function.

Integral probability metrics (IPM) [31] is a class of distance measures on probabilities that measures the largest discrepancy in expectation over a class of witness functions, which is defined as

$$d(P, Q) = \sup_{f \in \mathcal{F}} \left| \int f dP - \int f dQ \right| \quad (\text{A.4})$$

where P, Q are two probabilities and \mathcal{F} is a class of real-valued bounded measurable functions. Examples of such distances are shown in table A.3; in the table, $\|f\|_L$ is the Lipschitz semi-norm of a bounded continuous real-valued function f

$$\|f\|_L := \sup \left\{ \frac{|f(x) - f(y)|}{|x - y|} : x \neq y \right\} \quad (\text{A.5})$$

\mathcal{F}	Description	Note
$\{f : \ f\ _L \leq 1\}$	Kantorovich metric	The dual representation of the Wasserstein distance
$\{f : \ f\ _L + \ f\ _\infty \leq 1\}$	Dudley metric	
$\{f : \ f\ _\infty \leq 1\}$	L_1 distance Total variation metric $\times 2$	Equivalent to $\int P(dx) - Q(dx) $. The only nontrivial metric that belongs to f -divergence and IPM
$\{\mathbf{1}_{(-\infty, t]} : t \in \mathbb{R}^d\}$	Kolmogorov distance	
$\{f : \ f\ _{\mathcal{H}} \leq 1\}$	Kernel distance	\mathcal{H} represents a reproducing kernel Hilbert space (RKHS)

Table A.3: Examples of IPM [32].

The maximum mean discrepancy belongs to the kernel distance,

$$d(P, Q) = \sup_{f \in \mathcal{F}} (\mathbb{E}_{x \sim P} f(x) - \mathbb{E}_{y \sim Q} f(y)) \quad (\text{A.6})$$

When $\mathcal{F} = C^0(\mathcal{X})$, i.e., the set of all continuous, bounded functions on \mathcal{X} [33], we have $d(P, Q) = 0$ if and only if $P = Q$ and thus it can be used as a metric for proximity of P and Q . Such functions can be approximated with functions in a universal reproducing kernel Hilbert space [34]. The latter metric is used to design MMD GAN [35].

Optimal transport (OT) [36] can also be used to derive probability metrics. It basically considers the cost of transforming one probability distribution to another. Let \mathcal{X} and \mathcal{Y} be two measurable space. P, Q are two probability distributions on \mathcal{X} and \mathcal{Y} respectively. The Kantorovich problem in optimal transport is

$$\min_{\pi} \int c(x, y) d\pi(x, y) \quad (\text{A.7})$$

$$s.t. P_{\mathcal{X}\#}\pi = P \quad P_{\mathcal{Y}\#}\pi = Q \quad (\text{A.8})$$

where $P_{\mathcal{X}\#\pi}$ and $P_{\mathcal{Y}\#\pi}$ denotes the marginals of π with respect to the first and second component. If $\mathcal{X} = \mathcal{Y}$, and let $d(x, y)$ be a distance on the space \mathcal{X} . If $c(x, y) = d(x, y)^p$, $p \geq 1$ in eq. (A.7), the p -Wasserstein distance on \mathcal{X} is defined as

$$d(P, Q) = \left(\min_{\mu \in \mathcal{L}(P, Q)} \int c(x, y)^p d\pi(x, y) \right)^{1/p} \quad (\text{A.9})$$

where $\mathcal{L}(P, Q)$ is the set of all measures with marginals P and Q , and $\rho \geq 0$ is the cost function. For example, if $\mathcal{X} = \mathbb{R}^n$, we can pick $d(x, y) = |x - y|$. Different from many divergences, the Wasserstein distance is a true distance, i.e., $d(x, y) = d(y, x)$ and satisfies the triangle inequality. When $p = 1$, the 1-Wasserstein distance has a supremum form due to Kantorovich-Rubinstein duality

$$d(P, Q) = \sup_{\|f\|_L \leq 1} \mathbb{E}_{x \sim P}[f(x)] - \mathbb{E}_{x \sim Q}[f(x)] \quad (\text{A.10})$$

where $\|f\|_L \leq 1$ indicates f is 1-Lipschitz. The 1-Wasserstein distance is adopted in Wasserstein GAN [11].

Good performance in one metric does not necessarily mean the same in another metric. One would pick an appropriate metric for her specific applications. Also the choice of metrics has significant impact on the optimization algorithm. As an illustration, table A.4 shows the probability metric for two delta distribution and two Gaussian distributions. If we are comparing discrete distributions and we are using KL-divergence, JS-divergence or the total variation metric, we may get a constant or infinity number, and consequently the gradients will be meaningless.

Metrics	$P = \delta_{\theta_1}, Q = \delta_{\theta_2}$
KL-divergence	$+\infty$
JS-divergence	$\log 2$
Wasserstein-2 distance	$ \theta_1 - \theta_2 $
Total variation distance	1
IPM $\mathcal{F} = \{x, x^2\}$	$\max\{ \theta_1, \theta_2 , \theta_1^2 - \theta_2^2 \}$

Table A.4: Different probability metrics for two delta distribution. Here $\theta_1 \neq \theta_2$

References

References

- [1] H. Daniels, The asymptotic efficiency of a maximum likelihood estimator, in: Fourth Berkeley Symposium on Mathematical Statistics and Probability, Vol. 1, University of California Press Berkeley, 1961, pp. 151–163.
- [2] H. Cramér, Mathematical methods of statistics, Vol. 9, Princeton university press, 1999.

- [3] L. Le Cam, et al., On the asymptotic theory of estimation and testing hypotheses, in: Proceedings of the Third Berkeley Symposium on Mathematical Statistics and Probability, Volume 1: Contributions to the Theory of Statistics, The Regents of the University of California, 1956.
- [4] D. M. Blei, A. Kucukelbir, J. D. McAuliffe, Variational inference: A review for statisticians, *Journal of the American Statistical Association* 112 (518) (2017) 859–877.
- [5] M. Dashti, A. M. Stuart, The bayesian approach to inverse problems, *Handbook of Uncertainty Quantification* (2016) 1–118.
- [6] D. Van Ravenzwaaij, P. Cassey, S. D. Brown, A simple introduction to markov chain monte-carlo sampling, *Psychonomic bulletin & review* 25 (1) (2018) 143–154.
- [7] A. G. Baydin, B. A. Pearlmutter, A. A. Radul, J. M. Siskind, Automatic differentiation in machine learning: a survey, *Journal of Machine Learning Research* 18 (2018) 1–43.
- [8] K. Kládívko, Maximum likelihood estimation of the cox-ingersoll-ross process: the matlab implementation, *Technical Computing Prague* 7 (2007).
- [9] C. Anderson, R. E. Schumacker, A comparison of five robust regression methods with ordinary least squares regression: Relative efficiency, bias, and test of the null hypothesis, *Understanding Statistics: Statistical Issues in Psychology, Education, and the Social Sciences* 2 (2) (2003) 79–103.
- [10] I. Goodfellow, J. Pouget-Abadie, M. Mirza, B. Xu, D. Warde-Farley, S. Ozair, A. Courville, Y. Bengio, Generative adversarial nets, in: *Advances in neural information processing systems*, 2014, pp. 2672–2680.
- [11] M. Arjovsky, S. Chintala, L. Bottou, Wasserstein gan, *arXiv preprint arXiv:1701.07875* (2017).
- [12] S. Nowozin, B. Cseke, R. Tomioka, f-gan: Training generative neural samplers using variational divergence minimization, in: *Advances in neural information processing systems*, 2016, pp. 271–279.
- [13] D. P. Kingma, J. Ba, Adam: A method for stochastic optimization, *arXiv preprint arXiv:1412.6980* (2014).
- [14] G. Hinton, N. Srivastava, K. Swersky, Lecture slides, https://www.cs.toronto.edu/~tijmen/csc321/slides/lecture_slides_lec6.pdf, (Accessed on 04/01/2019).
- [15] A. Skajaa, Limited memory bfgs for nonsmooth optimization, Master’s thesis (2010).
- [16] A. Jolicoeur-Martineau, Gans beyond divergence minimization, *arXiv preprint arXiv:1809.02145* (2018).
- [17] I. Goodfellow, Nips 2016 tutorial: Generative adversarial networks, *arXiv preprint arXiv:1701.00160* (2016).
- [18] I. J. Myung, Tutorial on maximum likelihood estimation, *Journal of mathematical Psychology* 47 (1) (2003) 90–100.
- [19] A. Ly, M. Marsman, J. Verhagen, R. P. Grasman, E.-J. Wagenmakers, A tutorial on fisher information, *Journal of Mathematical Psychology* 80 (2017) 40–55.
- [20] C.-S. Chou, H.-J. Lin, Some properties of cir processes, *Stochastic analysis and applications* 24 (4) (2006) 901–912.
- [21] A. Rinaldo, Lecture notes, http://www.stat.cmu.edu/~arinaldo/Teaching/36752/S18/Scribed_Lectures/Apr5.pdf.
- [22] G. H. Golub, C. F. Van Loan, *Matrix computations*, Vol. 3, JHU press, 2012.
- [23] P. Glasserman, B. Yu, Large sample properties of weighted monte carlo estimators, *Operations Research* 53 (2) (2005) 298–312.
- [24] D. G. Luenberger, et al., *Investment science*, OUP Catalogue (1997).
- [25] A. L. Gibbs, F. E. Su, On choosing and bounding probability metrics, *International statistical review* 70 (3) (2002) 419–435.
- [26] G. E. Crooks, On measures of entropy and information, *Tech. Note* 9 (2017) v4.
- [27] T. M. Cover, J. A. Thomas, *Elements of information theory*, John Wiley & Sons, 2012.
- [28] B. Yu, Tutorial: Information theory and statistics, <https://www.icmla-conference.org/icmla08/slides1.pdf>, (Accessed on 05/05/2019) (2008).
- [29] J. Lin, Divergence measures based on the shannon entropy, *IEEE Transactions on Information theory* 37 (1) (1991) 145–151.
- [30] X. Mao, Q. Li, H. Xie, R. Y. Lau, Z. Wang, S. Paul Smolley, Least squares generative adversarial

- networks, in: Proceedings of the IEEE International Conference on Computer Vision, 2017, pp. 2794–2802.
- [31] B. K. Sriperumbudur, K. Fukumizu, A. Gretton, B. Schölkopf, G. R. Lanckriet, On integral probability metrics, ϕ -divergences and binary classification, arXiv preprint arXiv:0901.2698 (2009).
 - [32] B. K. Sriperumbudur, K. Fukumizu, A. Gretton, B. Schölkopf, G. R. Lanckriet, et al., On the empirical estimation of integral probability metrics, *Electronic Journal of Statistics* 6 (2012) 1550–1599.
 - [33] R. M. Dudley, *Real analysis and probability*, Chapman and Hall/CRC, 2018.
 - [34] I. Steinwart, On the influence of the kernel on the consistency of support vector machines, *Journal of machine learning research* 2 (Nov) (2001) 67–93.
 - [35] C.-L. Li, W.-C. Chang, Y. Cheng, Y. Yang, B. Póczos, Mmd gan: Towards deeper understanding of moment matching network, in: *Advances in Neural Information Processing Systems*, 2017, pp. 2203–2213.
 - [36] G. Peyré, M. Cuturi, et al., Computational optimal transport, *Foundations and Trends® in Machine Learning* 11 (5-6) (2019) 355–607.